Strain mapping at nanometer resolution using advanced nano-beam electron diffraction

V. B. Ozdol[1*], C. Gammer[1,2,3*+], X. G. Jin[4], P. Ercius[1], C. Ophus[1], J. Ciston[1] and A. M. Minor[1,2+]

[1]National Center for Electron Microscopy, Molecular Foundry, Lawrence Berkeley National Laboratory, Berkeley, CA 94720, USA

[2]Department of Materials Science and Engineering, University of California, Berkeley, CA 94720, USA

[3]Physics of Nanostructured Materials, Faculty of Physics, University of Vienna, 1090 Vienna, Austria

[4]Institute for Advanced Research, Nagoya University, Nagoya 464-8603, Japan

* The authors contributed to this work equally and share the first authorship.

+ corresponding authors christoph.gammer@univie.ac.at, aminor@lbl.gov

We report on the development of a nanometer scale strain mapping technique by means of scanning nano-beam electron diffraction. Only recently possible due to fast acquisition with a direct electron detector, this technique allows for strain mapping with a high precision of 0.1 % at a lateral resolution of 1 nm for a large field of view (FOV) reaching up to 1 µm. We demonstrate its application to a technologically relevant strain-engineered GaAs/GaAsP hetero-structure and show that the method can even be applied to highly defected regions with substantial changes in local crystal orientation. Strain maps derived from atomically resolved scanning transmission electron microscopy images were used to validate the accuracy, precision and resolution of this versatile technique.

Strain engineering of semiconductors has become an important method for altering the structural, electronic and optical properties of materials[1]. Today's microprocessors for instance utilize strained silicon channels to enhance the charge carrier mobility[2]. Strain-induced polarization fields in Group III-V quantum well structures play an important role in the emission characteristics of light emitting diodes[3]. Strain compensated super-lattice structures are used to improve crystal growth and achieve higher quantum efficiencies in photocathode diodes[4]. The continuous scaling of the active regions of these devices requires characterization techniques with nanometer scale resolution to assist the development of new material processing methods.

Among the various techniques that can be used to measure strain such as X-ray[5] and neutron[6] diffraction or Raman spectroscopy[7], transmission electron microscopy (TEM) is the only tool capable of measuring strain at the nanometer scale[8]. Convergent-beam electron diffraction (CBED)[9] provides high precision but requires comparison with simulations to analyze the complex patterns and compensate for sample thickness. Furthermore, the sample must be oriented along a high order zone axis making it unsuitable for most of the device designs due to interface broadening. Conventional nano-beam electron diffraction (NBED)[10] using a parallel beam is quite versatile and experimentally easy to apply at low spatial resolution on the order of 3 nm, mainly limited by the beam size. Previously, NBED was mainly limited by the slow acquisition speeds of conventional CCD cameras used to acquire the diffraction patterns and is mostly suitable for one-dimensional strain profiling. Combining precession electron diffraction (PED) with NBED results in more symmetric and pseudo-kinematical diffraction patterns. This leads to an improved precision but can increase the obtainable spot size due to aberrations in the condenser

lenses and objective pre-field. Recently a resolution of 2.5 nm measured from the full width half-maximum (FWHM) of the beam was demonstrated for strain mapping with PED[11]. The resolution of NBED can be significantly improved using a more convergent beam[12] and the slow acquisition speeds of conventional CCD cameras can be overcome by using direct electron detectors[13], but the application of NBED to large fields-of-view has not been demonstrated.

High-resolution TEM (HRTEM)[14] coupled with image processing algorithms provides the necessary lateral resolution (better than 1 nm); however, the technique relies on extremely precise measurements of atomic column positions which requires high quality, thin specimens and delicately controlled imaging conditions. Recent improvements in the stability of TEMs and the introduction of aberration-correctors allows high-resolution scanning TEM (HRSTEM)[15] to be used for strain mapping. STEM provides directly interpretable image contrast to locate atomic column intensities and is less sensitive to sample thickness or surface damage but image distortions due to scan coil misalignments and sample drift can limit the precision and FOV. However, recently it was shown that the use of multiple images and correction of the drift and scan distortions can increase the achievable FOV for HRSTEM[16]. Dark-field electron holography (DFEH) techniques, either off-axis[17] or in-line[18] provide a larger FOV reaching up to 1 μm but require a dedicated microscope equipped with an electrostatic bi-prism or a sophisticated focal series reconstruction algorithm, respectively. In addition, both HRSTEM and holographic techniques require the sample to be in exact zone axis or two-beam diffracting condition and to have exactly the same orientation throughout the entire analyzed area. Inherently, this last requirement limits the FOV and types of samples that can be analyzed.

In the present work, we apply NBED in the scanning mode to overcome the spatial and temporal limitations of existing methods to enable practical strain mapping. We use a direct electron detector to acquire diffraction patterns one order of magnitude faster than conventional CCD imaging in combination with an efficient evaluation algorithm to achieve a straightforward and precise method for determining the strain field of large areas of any sample with high spatial resolution. Each scan position provides a direction measurement of the local strain from the diffraction pattern without the need to compare with neighboring regions. Thus, drift and other scanning distortions do not affect the strain measurements. The sample studied here was extracted from a high-efficiency photocathode device[19], which consists of GaAs/GaAsP super-lattice (SL) grown on a AlGaAsP virtual substrate that was grown on (001) GaP substrate. Cross-sectional wedge TEM specimens were prepared by automated mechanical polishing (Allied MultiPrep) followed by low energy Argon ion milling in a cooled stage (Gatan PIPS 2) (200 eV, -150 C°) to minimize the ion beam-induced surface damage. HRSTEM and NBED experiments were performed using TEAM I, an ultra-stable FEI Titan 80-300[20] equipped with a high-brightness field emission gun (FEG) operated at 300 kV. The high-angle annular dark field (HAADF) STEM image (acquired with a semi-convergence angle of 17 mrad and semi-collection angles 50-270 mrad) shown in Figure 1(a) reveals that the entire active device region consisting of 90 pairs of SL with nominal 4.0 ± 0.3 nm layer thickness. Although SL exhibits monolayer thickness fluctuations, the interfaces are sharp and coherent as shown in Figure 1(b). The lattice mismatch between the AlGaAsP layer and the coherently grown GaAsP/GaAs SL results in alternating tetragonal out-of-plane (ε_{yy}) compressive and tensile strain, respectively. In such a structure, an opposing strain is introduced in the barrier layers to offset the strain in

the quantum well layers so that no critical thickness limitation exists on the overall thickness of the SL structure. It has been reported that a GaAs/GaAsP strain-compensated SL could provide a high spin-polarization of over 90%[4].

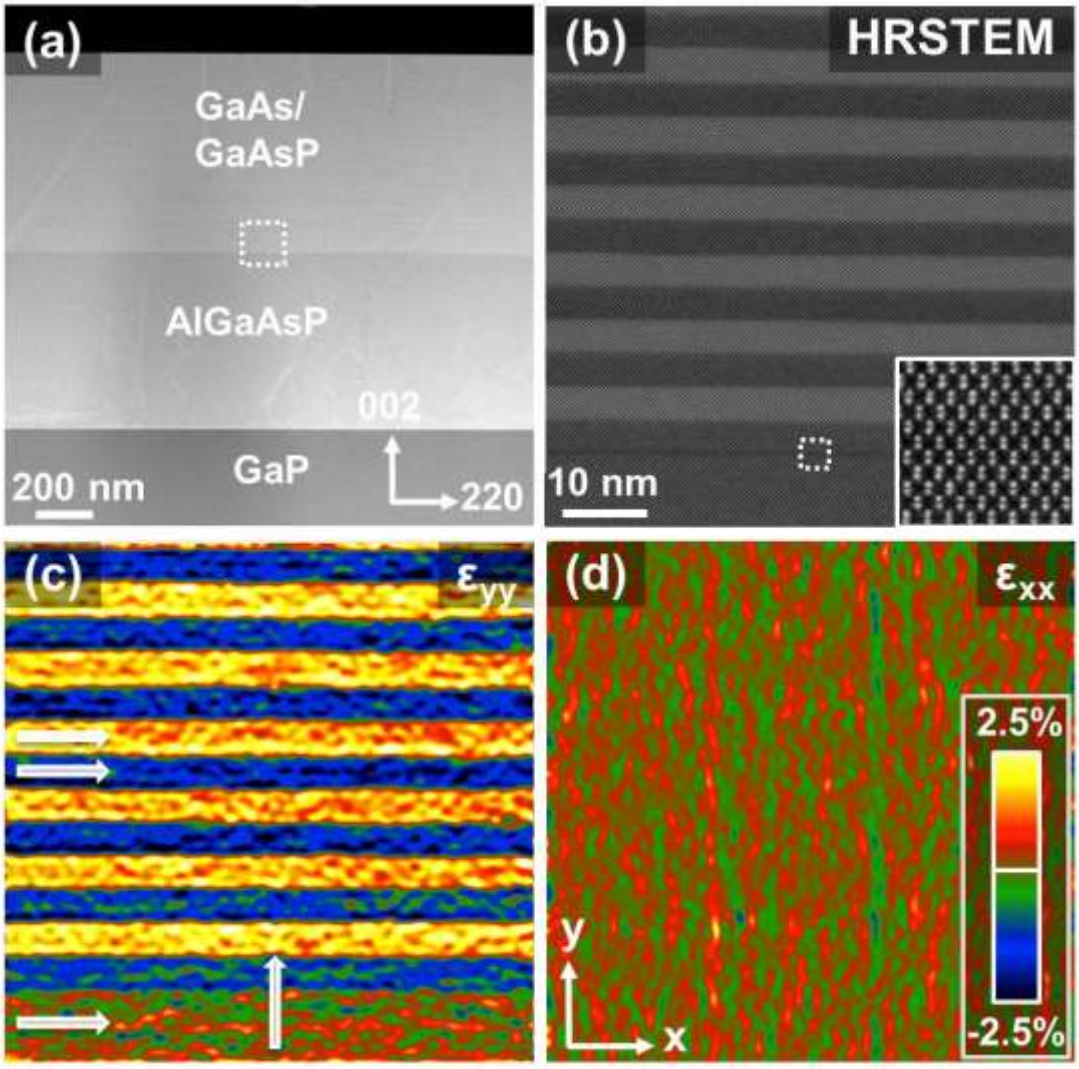

FIG. 1 HRSTEM analysis of GaAs/GaAsP multilayer device cross-section. (a) Low magnification image of GaP substrate, AlGaAsP virtual substrate and GaAs/GaAsP multilayer. (b) Atomic-resolution HRSTEM image of boxed region in (a). The insert shows the image at real pixel resolution. The dumbells with a spacing of 1.4 A are clearly resolved. (c) GPA map from HRSTEM data of ε_{yy} strain where y is the [002] direction. (d) GPA map from HRSTEM data of ε_{xx} strain where x is the [220] direction.

We first investigated the strain state of the hetero-structure using atomic-resolution HAADF-STEM coupled with geometric phase analysis (GPA)[14,21]. Figure 1(b) displays the HRSTEM image of the bottom part of the active device

region. Color-coded two dimensional out-of-plane (ε_{yy}) and in-plane (ε_{xx}) strain maps with 1.2 nm spatial resolution are shown in Figure 1(c) and (d), respectively. Here, the AlGaAsP layer is defined as an unstrained reference. As expected from the coherent epitaxial growth, the in-plane strain values across the hetero-structure with respect to the reference region are zero.

The HRSTEM-based strain mapping technique as shown in Figure 1 requires that the atomic columns are resolved across the entire region of interest, a requirement that typically limits the available FOV to 100 nm mostly due to sample drift. Most of today's strain engineered semiconductor devices however contain active device regions extending beyond the limited FOV of high-resolution imaging. The photocathode device investigated here for instance consists of a 720 nm thick SL structure. To overcome this limitation we have exploited scanning NBED in combination with the capabilities of a fast direct electron detector. Figure 2(a) shows an annular dark field (ADF) STEM image recorded with an inner semi-collection angle of 20 mrad of the same region as the region characterized using HRSTEM-GPA. The image was acquired in the microprobe mode of the TEAM I microscope where the three independent condenser lenses were used to form a sub-nanometer diameter electron probe with a semi-convergence angle of 2.8 mrad using a 40 μm condenser aperture at 300 kV. For each individual beam position in the 256x256 STEM scan

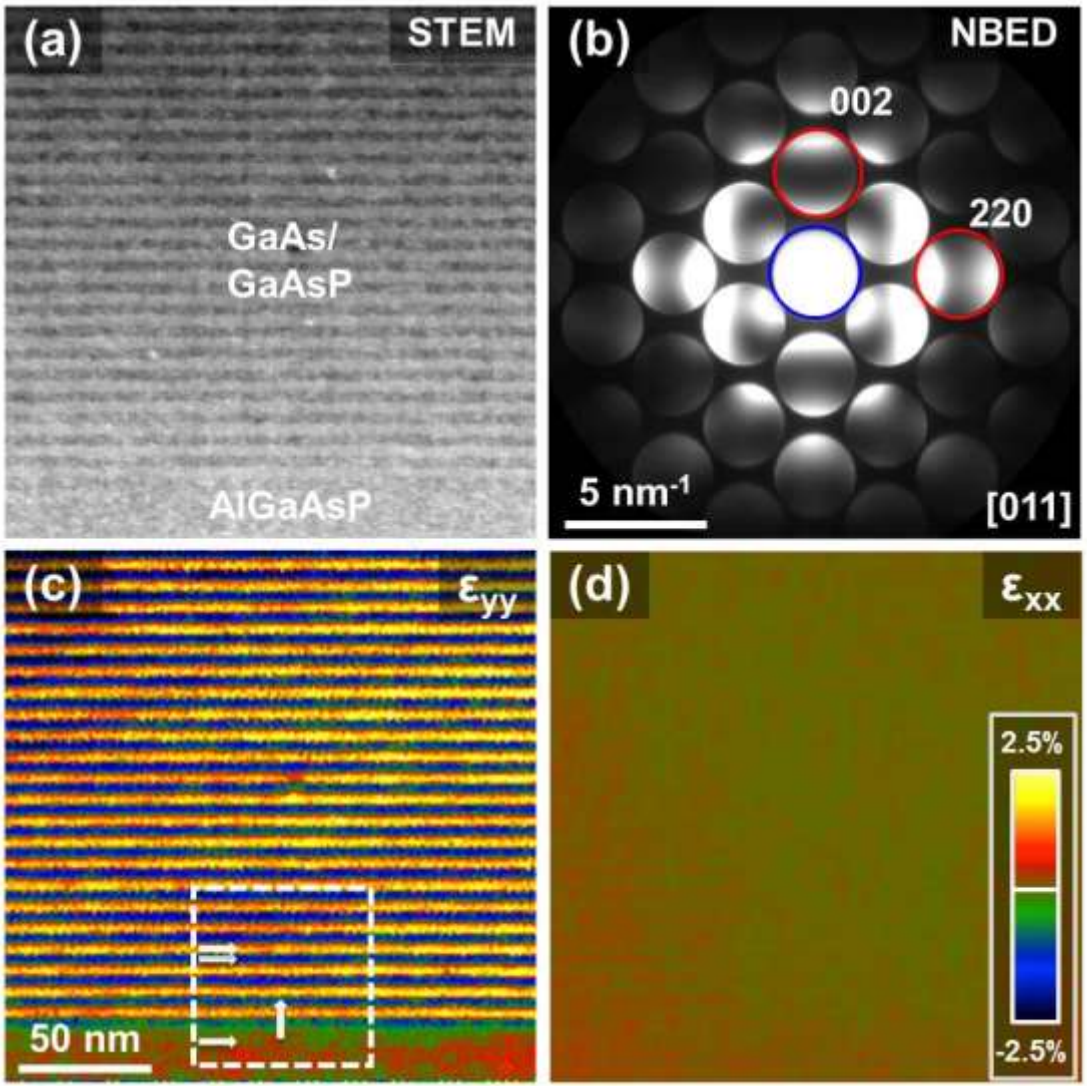

FIG 2. NBED analysis of GaAs/GaAsP multilayer device cross-section. (a) HAADF image of the analyzed section. (b) representative nanodiffraction pattern taken from the dataset with the [200] and [220] diffraction vectors that were analyzed for the strain analysis highlighted. (c) NBED strain map of ε_{yy} strain where y is the [002] direction. The region of the device analyzed by HRSTEM in Figure 1 is noted by the white box. (d) NBED strain map of ε_{xx} strain where x is the [220] direction.

NBED patterns were recorded simultaneously using a Gatan K2-IS direct detector at a frame rate of 400 f/s in relatively fast total acquisition time of 160 s. Figure 2(b) displays the integrated diffraction pattern reconstructed from the 4D data cube consisting of 65500 images with 1920 pixels x 1792 pixels. To calculate the strain from the diffraction patterns, a robust pattern recognition algorithm was implemented

in Digital Micrograph (Gatan Inc.). First, a mask was created from the shape of the central CBED disk and modified to have an intensity distribution proportional to the inverse distance from the spot center. This weighted the mask more heavily to detect edges. This mask was used to measure the locations of the central spot and several diffracted spots by squared cross-correlation with sub-pixel precision. Details on the cross-correlation procedure are given in supplemental Figure S1[22]. The relative distances between the central spot and diffracted spots are a direct measurement of the local strain at each beam position. The AlGaAsP layer was set as a reference and therefore used to define the unstrained diffraction vectors $g_i^{unstrained}$. Subsequently, for each diffraction pattern the transformation matrix T was computed from the diffraction vectors g_i using $g_i = T\, g_i^{unstrained}$. The transformation T matrix was separated into a rotation matrix R and a symmetric strain matrix U using polar decomposition $T=RU$ [23]. The planar strains were computed by $\varepsilon_{xx}=1-U_{00}$ and $\varepsilon_{yy}=1-U_{11}$ and the shear and rotation can be compute using $\varepsilon_{xy}=1-R_{01}$ and $\theta=cos^{-1}R_{00}$. The resulting color-coded 2D out-of-plane (ε_{yy}) and in-plane (ε_{xx}) strain maps are shown in Figure 2(c) and (d) where the AlGaAsP layer defined as a reference. The resolution of the strain maps as defined by the step size is 0.8 nm at a FOV of 200 nm. The beam size was well below 1 nm and therefore does not limit the resolution in the present case. As a comparison, the FOV achieved with HRSTEM is indicated with a dashed box in Figure 2(c), demonstrating the increase in FOV. It is notable that the strain maps are presented unfiltered and unsmoothed.

Figure 3 quantitatively compares the two strain mapping methods. The HRSTEM-GPA profile scans within the two adjacent layers (as marked with white arrows in Figure 1(c)) revealed average strain values of 1.1 ± 0.3 % and -1.3 ± 0.4 % without remarkable strain fluctuations (cf. Figure 3(a)). The standard deviation of the

variations inside the reference area, which defines the inherent noise of the GPA is calculated as 0.3 % and is comparable with the fluctuations within the layers. Profile scans from the scanning NBED strain maps within the same two adjacent layers (as marked with white arrows in Figure 2(c)) revealed average strain values of 1.1 ± 0.2 % and -1.2 ± 0.2 %, respectively (cf. Figure 3(a)) in excellent agreement with the HRSTEM results. The standard deviation of the variations inside the reference area was determined to be 0.1 %, showing an improved precision as compared to the results achieved by HRSTEM-GPA. In addition to the profile scans within the adjacent layers, a profile scan across the layers was carried out at a location shown in Figures 1(c) and 2(c). Figure 3(b) shows the comparison of the scans obtained by HRSTEM-GPA and by NBED, showing excellent agreement.

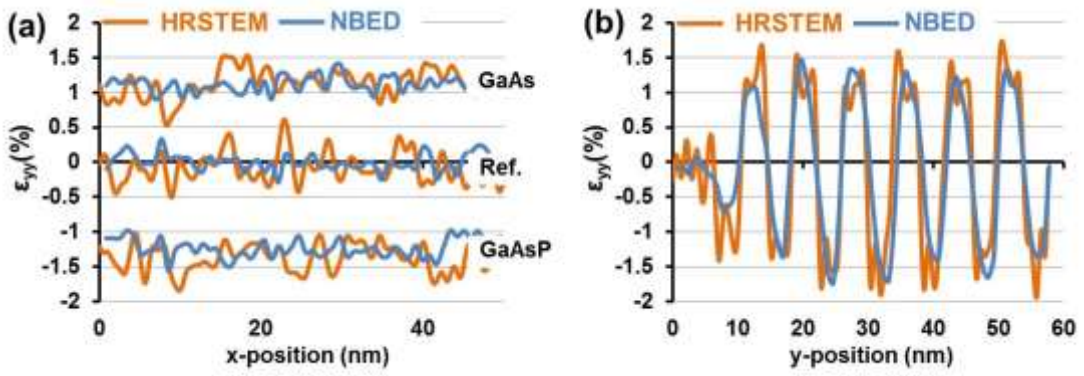

FIG. 3 Quantitative comparison of HRSTEM vs. NBED analysis. (a) Profile scans (ε_{yy}) of the 3 different layers analyzed in the in-plane direction. (b) Profile scans (ε_{yy}) in the out-of-plane direction.

In addition to analyzing a perfect region of the hetero-structure, scanning NBED strain mapping was performed on a highly defected region to demonstrate the robustness of the technique. Figure 4(a) shows the ADF-STEM image (inner semi-collection angle 20 mrad) of an area containing multiple defects. In addition to defect structures, the relatively large FOV has a change in orientation (a mistilt)

demonstrated with CBED patterns from the white boxes labeled 1 and 2. It is impossible to analyze the same area using a technique such as HRSTEM-GPA. From the NBED diffraction patterns acquired for each individual pixel shown in the HAADF image (512 positions x 512 positions), a strain map was calculated having a resolution of 2 nm and a FOV reaching up to 1 µm.

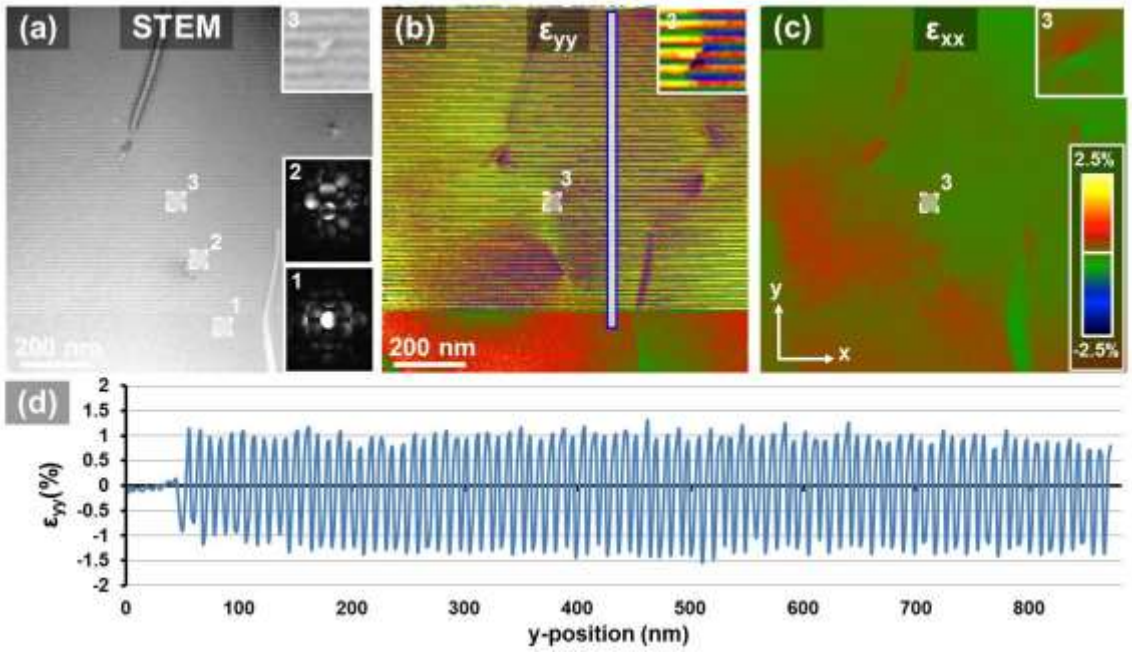

FIG. 4 NBED analysis of GaAs/GaAsP multilayer device cross-section across a large 1µm FOV. (a) HAADF image of the analyzed section. Inset are CBED patterns taken from areas 1 and 2 showing the misorientation possible to analyze with the technique. Inset labeled 3 is a short-range stacking fault. (b) NBED strain map of ε_{yy} strain where y is the [002] direction. (c) NBED strain map of ε_{xx} strain where x is the [220] direction. (d) a ε_{yy} profile scan across the entire device as indicated by the vertical box in (b).

The resulting color-coded 2D out-of-plane (ε_{yy}) and in-plane (ε_{xx}) strain maps are shown in Figure 4(b) and (c), respectively. In addition to the strain oscillations between the multilayers, strain-fields around the dislocations are visible. The strain field around an individual short-range stacking fault, as indicated by a white box labeled 3, is shown as inset. Figure 4(d) shows a profile scan across the whole active device region (indicated in Figure 4(b)). While in the case of HRSTEM-GPA only 6

pairs of SL were imaged, here we measured all 90 SL pairs of the device, revealing that the strains in the multilayers are very reproducible across the entire device. The results also demonstrate that using NBED high quality strain maps can be obtained even across a FOV that could not be analyzed in high resolution because of the change in orientation. Furthermore, the NBED technique does not require a high quality thin TEM specimen. Instead, the NBED technique can be optimized with a foil thickness that is thick enough to minimize the thin foil relaxation [24] but still thin enough to minimize loss of resolution due to beam-broadening in the sample. In the present case the sample thickness was estimated to be 40 nm by comparing averaged experimental NBED patterns with simulated ones[25], similar to the PACBED technique described by LeBeau et al.[26]. Multislice simulations show that the electron beam diameter increases by a factor of approximately 1.4 after propagating 40 nm. Details of the simulations, showing the simulated NBED pattern and a detailed analysis of the beam broadening dependence of sample thickness are shown in the supplemental Figures S2 and S3[22].

The dataset acquired by NBED contains very rich information on the local structure of the material. One example is the generation of arbitrary dark-field images from the datasets using virtual detectors[27,28]. A region is selected in the diffraction pattern and a dark-field image is formed by summing the corresponding intensity in the diffraction pattern for every raster position. Examples of virtual dark-field images generated for the area investigated in Figure 4 are shown in supplemental Figure S4[22].

In conclusion, we have shown that scanning NBED in combination with fast electron detectors is ideally suited to map strain with very high precision (+/- 0.1%), high spatial resolution (~1 nm), and a large FOV (~1 um) for high throughput characterization of strained materials. We have applied this technique to map strain

fields in GaAs/GaAsP SL structures and demonstrated its performance both for high-quality hetero-structures as well as for highly defected regions where existing techniques based on high-resolution or diffraction contrast would fail. In the case of the defect-free hetero-structure we have analyzed the same sample for comparison using aberration-corrected HRSTEM-GPA. The measurements agree very well within the error bars of the two techniques. It is important to note that the localized diffraction dataset generated by NBED contains extensive information about the sample that can be used for example to construct virtual dark-field images. The technique is also well adapted for simultaneous compositional analysis by means of energy dispersive X-ray spectroscopy[29] for more accurate assessment of the strain state. Importantly, the NBED technique does not rely on a FOV with a single well-aligned diffraction condition or zone axis orientation, therefore it can presumably be applied to other types of samples such as metals or polycrystalline structures, where an understanding of the strain on the nanoscale is often limited to model configurations due to experimental limitations posed by local mistilts in the material.

ACKNOWLEDGEMENTS

We acknowledge financial support from the Austrian Science Fund (FWF):[J3397] and the Molecular Foundry, Lawrence Berkeley National Laboratory, which is supported by the U.S. Dept. of Energy under Contract # DE-AC02-05CH11231. We thank Ulrich Dahmen for helpful discussion and Gatan, Inc. for technical support.

REFERENCES

[1] J. Li, Z. Shan, and E. Ma, MRS Bull. **39**, 108 (2014).

[2] M. Chu, Y. Sun, U. Aghoram, and S.E. Thompson, Annu. Rev. Mater. Res. **39**, 203 (2009).

[3] A.E. Romanov, T.J. Baker, S. Nakamura, and J.S. Speck, J. Appl. Phys. **100**, 023522 (2006).

[4] X. Jin, A. Mano, F. Ichihashi, N. Yamamoto, and Y. Takeda, Appl. Phys. Express **6**, 015801 (2013).

[5] E.J. Mittemeijer and U. Welzel, Z. Krist. **223**, 552 (2008).

[6] A. Krawitz and T.M. Holden, MRS Bull. **15**, 57 (1990).

[7] I. De Wolf and I. De Wolf, J. Raman Spectrosc. **883**, 877 (1999).

[8] M.J. Hÿtch and A.M. Minor, MRS Bull. **39**, 138 (2014).

[9] L. Clément, R. Pantel, L.F.T. Kwakman, and J.L. Rouvière, Appl. Phys. Lett. **85**, 651 (2004).

[10] K. Usuda, T. Numata, T. Irisawa, N. Hirashita, and S. Takagi, Mater. Sci. Eng. B Solid-State Mater. Adv. Technol. **124-125**, 143 (2005).

[11] Y.Y. Wang, D. Cooper, J. Rouviere, C.E. Murray, N. Bernier, and J. Bruley, Appl. Phys. Lett. **106**, 042104 (2015).

[12] K. Müller, A. Rosenauer, M. Schowalter, J. Zweck, R. Fritz, and K. Volz, Microsc. Microanal. **18**, 995 (2012).

[13] K. Müller, H. Ryll, I. Ordavo, S. Ihle, L. Strüder, K. Volz, J. Zweck, H. Soltau, and A. Rosenauer, Appl. Phys. Lett. **101**, 212110 (2012).

[14] M.J. Hÿtch, E. Snoeck, and R. Kilaas, Ultramicroscopy **74**, 131 (1998).

[15] D. Cooper, C. Le Royer, A. Béché, and J.L. Rouvière, Appl. Phys. Lett. **100**, 233121 (2012).

[16] A.A. Oni, X. Sang, S. V. Raju, S. Dumpala, S. Broderick, A. Kumar, S. Sinnott, S. Saxena, K. Rajan, and J.M. LeBeau, Appl. Phys. Lett. **106**, 011601 (2015).

[17] M. Hÿtch, F. Houdellier, F. Hüe, and E. Snoeck, Nature **453**, 1086 (2008).

[18] C.T. Koch, V.B. Özdöl, and P.A. Van Aken, Appl. Phys. Lett. **96**, 091901 (2010).

[19] X. Jin, B. Ozdol, M. Yamamoto, A. Mano, N. Yamamoto, and Y. Takeda, Appl. Phys. Lett. **105**, 203509 (2014).

[20] R. Erni, M.D. Rossell, C. Kisielowski, and U. Dahmen, Phys. Rev. Lett. **102**, 096101 (2009).

[21] Y. Zhu, C. Ophus, J. Ciston, and H. Wang, Acta Mater. **61**, 5646 (2013).

[22]*See Supplemental Material at [URL Will Be Inserted by AIP] for Supplemental Figures.* (n.d.).

[23] M. Negahban, *The Mechanical and Thermodynamical Theory of Plasticity* (CRC Press, Boca Raton, 2010).

[24] L. De Caro, A. Giuffrida, E. Carlino, and L. Tapfer, Acta Crystallogr. Sect. A Found. Crystallogr. **53**, 168 (1997).

[25] E. Kirkland, *Advanced Computing in Electron Microscopy*, Second Edi (Springer, New York, 2010).

[26] J.M. Lebeau, S.D. Findlay, L.J. Allen, and S. Stemmer, Ultramicroscopy **110**, 118 (2010).

[27] C. Gammer, V. Burak Ozdol, C.H. Liebscher, and A.M. Minor, Ultramicroscopy (2015).

[28] J. Tao, D. Niebieskikwiat, M. Varela, W. Luo, M.A. Schofield, Y. Zhu, M.B. Salamon, J.M. Zuo, S.T. Pantelides, and S.J. Pennycook, Phys. Rev. Lett. **103**, 097202 (2009).

[29] P. Schlossmacher, D. Klenov, B. Freitag, and H.S. von Harrach, Micros. Today **18**, 14 (2010).

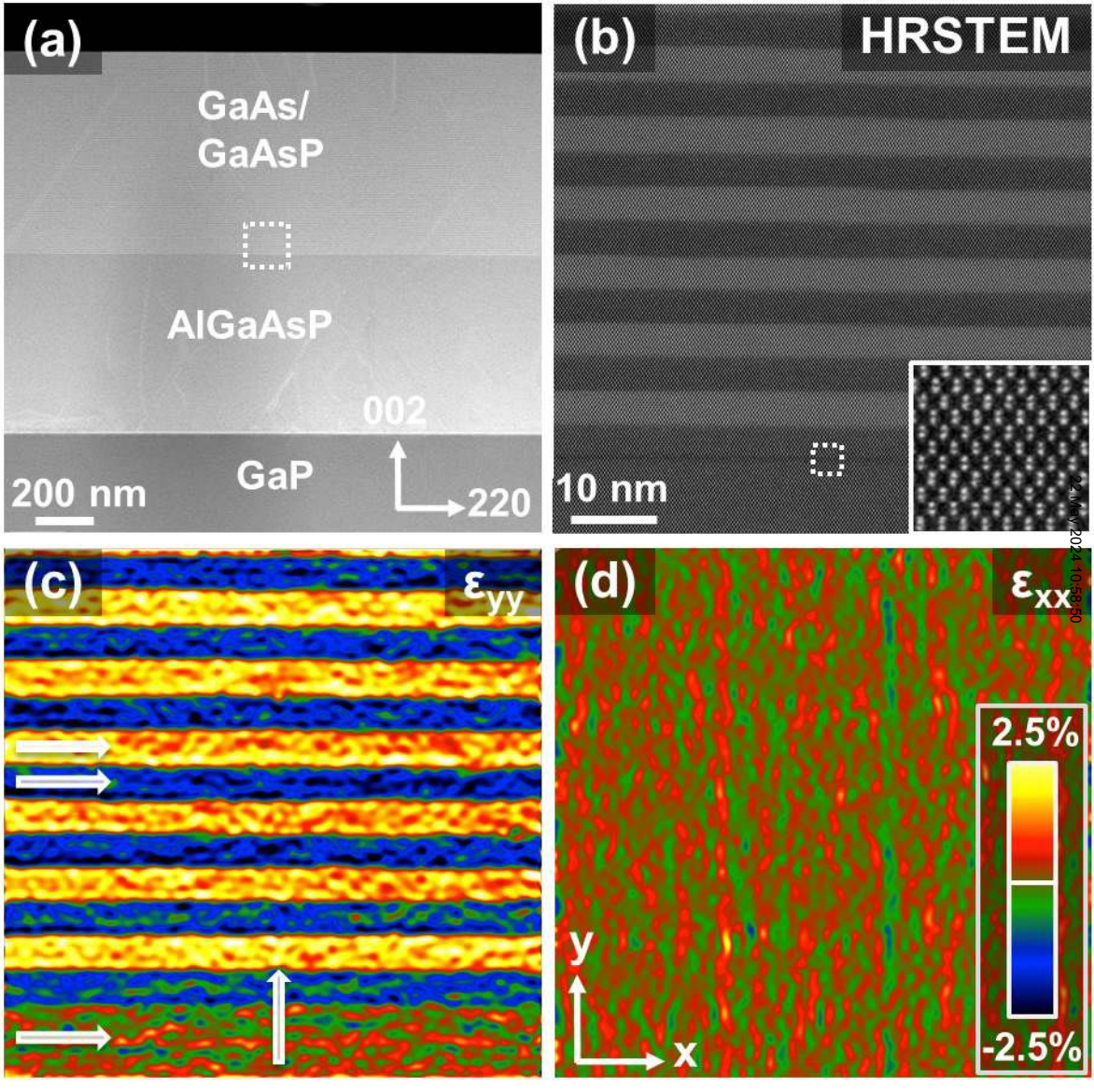
(a)
GaAs/
GaAsP
AlGaAsP
002
GaP
200 nm
220
(b)
HRSTEM
10 nm
(c)
ε_{yy}
(d)
ε_{xx}
2.5%
-2.5%
y
x

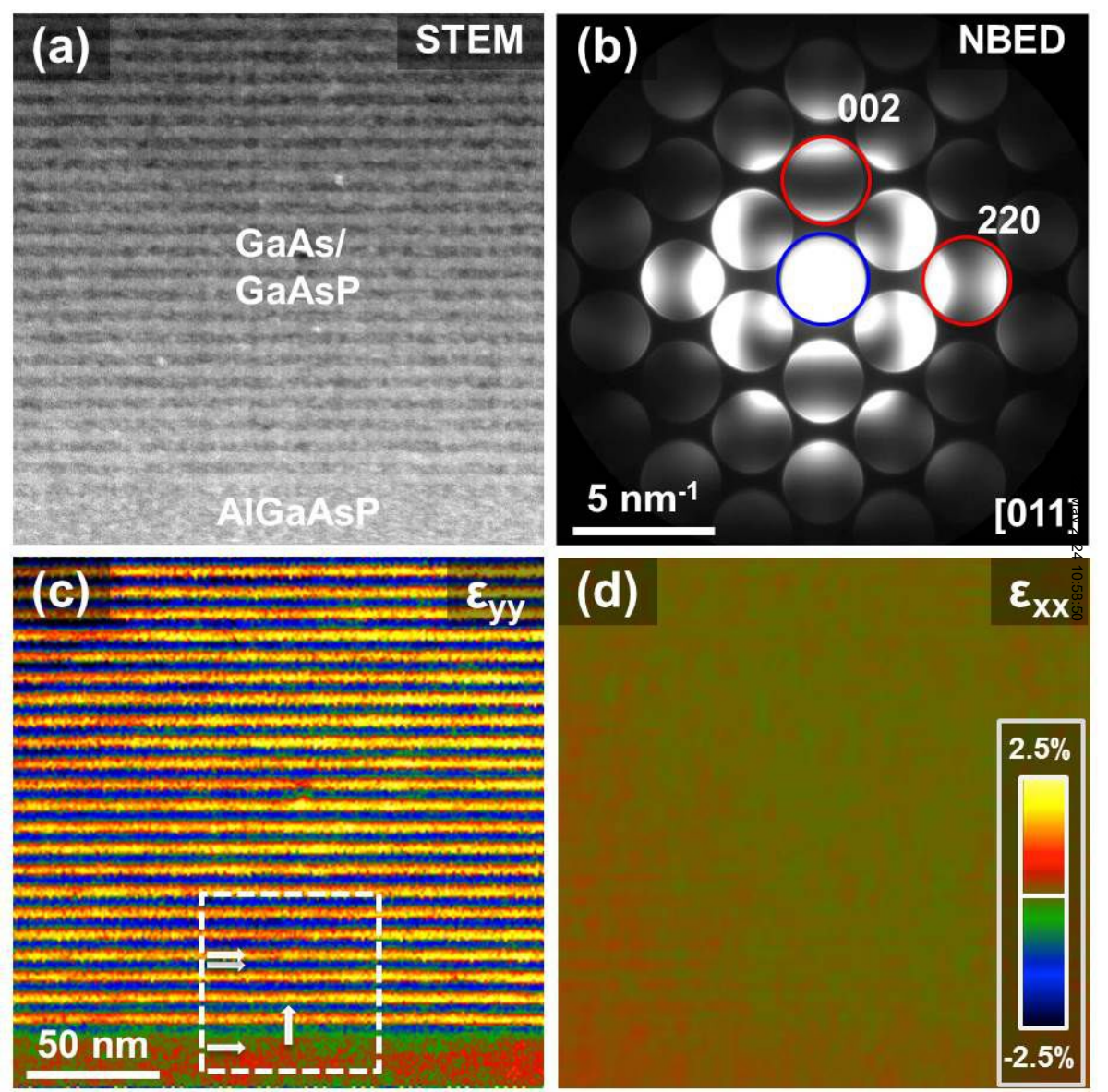
(a)
STEM
GaAs/
GaAsP
AlGaAsP
(b)
NBED
002
220
5 nm-1
[011]
(c)
εyy
50 nm
(d)
εxx
2.5%
-2.5%

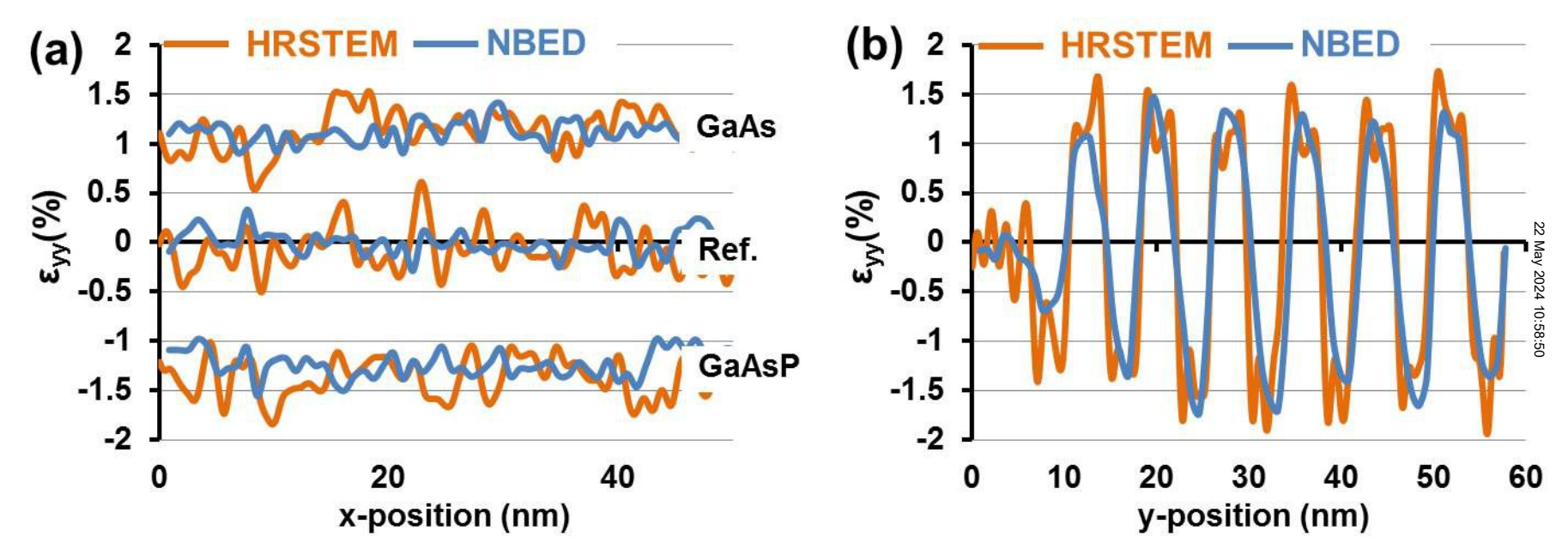
(a)
HRSTEM
NBED
GaAs
Ref.
GaAsP
ε_{yy}(%)
x-position (nm)
(b)
HRSTEM
NBED
ε_{yy}(%)
y-position (nm)
22 May 2024 10:58:50

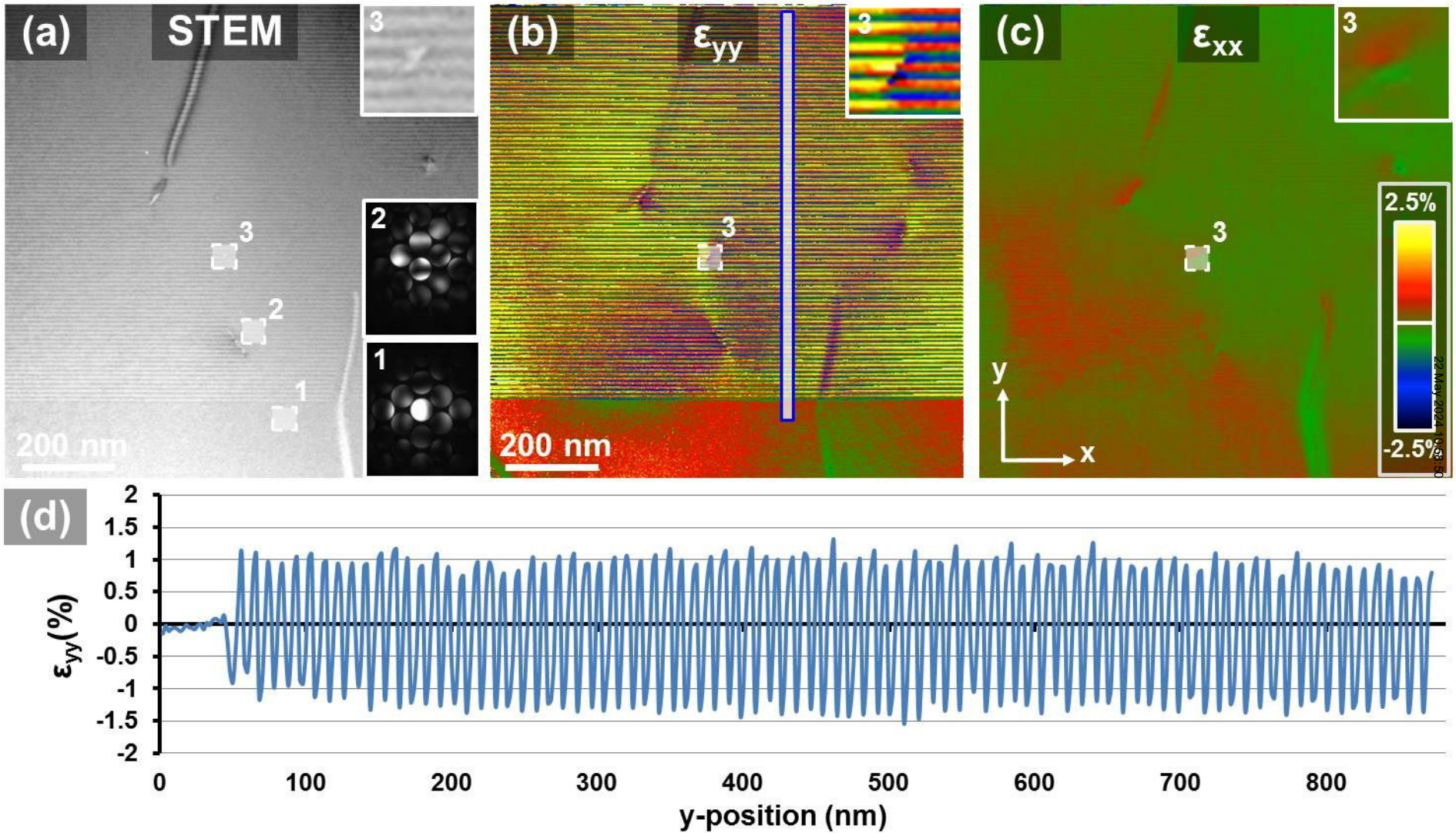
(a)
STEM
3
2
1
200 nm
(b)
ε_{yy}
3
200 nm
(c)
ε_{xx}
3
2.5%
-2.5%
y
x
(d)
ε_{yy}(%)
2
1.5
1
0.5
0
-0.5
-1
-1.5
-2
0
100
200
300
400
500
600
700
800
y-position (nm)